



Realization of semiconducting layered multiferroic heterojunctions via asymmetrical magnetoelectric coupling

Baishun Yang ^{1,2} Bin Shao,^{1,2} Jianfeng Wang,¹ Yang Li,¹ ChiYung Yam ^{1,2} Shengbai Zhang,³ and Bing Huang^{1,4,*}

¹Beijing Computational Science Research Center, Beijing 100193, China

²Shenzhen JL Computational Science and Applied Research Institute, Shenzhen 518109, China

³Department of Physics, Applied Physics and Astronomy, Rensselaer Polytechnic Institute, Troy, New York 12180, USA

⁴Department of Physics, Beijing Normal University, Beijing 100875, China



(Received 7 September 2020; revised 10 February 2021; accepted 12 May 2021; published 21 May 2021)

Two-dimensional (2D) semiconducting multiferroics that can effectively couple magnetic and polarization (P) orders have great interest for both fundamental research and technological applications in nanoscale, which are, however, rare in nature. In this paper, we propose a general mechanism to realize semiconducting 2D multiferroics via van der Waals (vdW) heterojunction engineering, as demonstrated in a typical heterostructure consisting of magnetic bilayer CrI_3 ($bi\text{-CrI}_3$) and ferroelectric monolayer In_2Se_3 . Interestingly, the novel indirect orbital coupling between Se $4p$ and Cr $3d$ orbitals, intermediated by the interfacial I $5p$ orbitals, is switchable in the opposite P configurations, resulting in an unexpected mechanism of strong asymmetrical magnetoelectric coupling. Therefore, along with the noticeable ferroelectric energy barrier induced by In_2Se_3 , the realization of opposite magnetic orders in opposite P configurations can eventually result in the novel multiferroicity in $bi\text{-CrI}_3/\text{In}_2\text{Se}_3$. Finally, we demonstrate that our mechanism can generally be applied to design other vdW multiferroics even with tunable layer thickness.

DOI: [10.1103/PhysRevB.103.L201405](https://doi.org/10.1103/PhysRevB.103.L201405)

Multiferroic materials that can simultaneously process more than one primary ferroic order in the same phase, including ferromagnetic (FM), ferroelectric (FE), or ferroelastic order [1–3], have attracted great attention for both scientific interest and technological applications [4,5]. In general, there are two types of multiferroics: type I has a weak magnetoelectric (ME) coupling because of the different FM and FE origins [6]; type II has a strong ME coupling, but the electric polarization (P) originated from the spin-orbital coupling is usually weak [7]. Meanwhile, the spontaneous P could be suppressed when a FE system is below its critical thickness, hindering their opportunities in nanoscale. Compared to the bulk FE systems, the two-dimensional (2D) layered FE systems with reduced surface energies may eliminate the intrinsic depolarization field in the monolayer (ML) limit [8,9]. Motivated by the discovery of 2D FE and magnetic systems [10–23], it is interesting to further explore the 2D multiferroics. Indeed, a few 2D systems, e.g., transition-metal (TM) halides [24], double-metal trihalides [25], and TM phosphorus chalcogenides [26,27] are predicted to be 2D single-phase multiferroics; however, in practice their artificially designed structures have so far prevented their realization (problem i).

Recently, the van der Waals (vdW) heterojunction engineering, via the stacking of layered systems with different properties, has provided a new opportunity to realize exotic physical properties and functionalities beyond those of their individual components [14,28,29]. Naturally, it is desirable to explore the feasibility of realizing vdW double-phase layered

multiferroics via the ME coupling of 2D magnetic and FE systems. Actually, several attempts have been made, e.g., for $\text{CrI}_3/\text{Sc}_2\text{CO}_2$ [30,31], $\text{FeI}_2/\text{In}_2\text{Se}_3$ [32], and $\text{MnCl}_3/\text{CuInP}_2\text{S}_6$ [33]. In these systems, an interface charge-transfer induced semiconductor to metal transition is required for achieving the magnetic ground-state switching under different P configurations, which, however, fundamentally eliminates their intrinsic semiconducting properties (problem ii).

In this paper, we propose a strategy of vdW heterojunction engineering of existing 2D systems to realize 2D semiconducting double-phase multiferroics, which can fundamentally overcome the above problems i and ii. Taking the prototype bilayer CrI_3 ($bi\text{-CrI}_3$)/ In_2Se_3 system as an example, the inclusion of ML FE In_2Se_3 induces a large FE energy barrier (E_b) into the system, which can effectively separate the different magnetic ground states, i.e., antiferromagnetic (AFM) and FM states, into opposite P configurations, i.e., $P\downarrow$ and $P\uparrow$. Importantly, the indirect coupling between the Se $4p$ and Cr $3d$ orbitals, mediated by the interfacial I $5p$ orbitals, is easily switchable in the opposite P configurations to result in a mechanism of strong asymmetrical ME coupling. In other words, the existence of the AFM- $P\downarrow$ and FM- $P\uparrow$ ground states, together with the large E_b , eventually results in the semiconducting multiferroic $bi\text{-CrI}_3/\text{In}_2\text{Se}_3$. Finally, we demonstrate that the mechanism is not system specific but can be generally applied to design other vdW multiferroics, even with tunable layer thickness.

The concept of the proposed vdW multiferroic heterojunction is illustrated in Fig. 1. Basically, it includes two components: a vdW semiconducting bilayer magnet ($bi\text{-magnet}$) [Fig. 1(a)] and a FE ML [Fig. 1(b)]. As shown in

*bing.huang@csrc.ac.cn

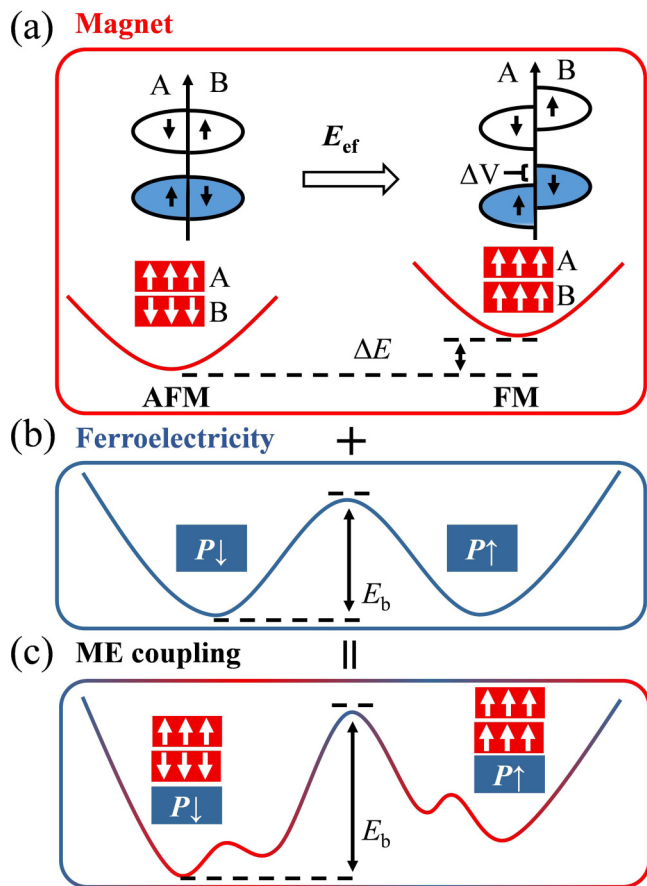


FIG. 1. Concept and schematic diagrams for realizing vdW multiferroics. (a) Electronic and magnetic states for a 2D bilayer magnet without (left panel) and with (right panel) an E_{ef} . Arrows denote spin orders in AB layers. (b) Ferroelectric double-well potential energy curve. $P\uparrow$ and $P\downarrow$ denote two opposite FE polarizations, while E_b is the energy barrier between the $P\uparrow$ and $P\downarrow$ states. (c) Realization of vdW multiferroics via an asymmetrical ME coupling between the bilayer magnet and ML FE systems.

Fig. 1(a), in the *bi*-magnet, its interlayer magnetic order could be either AFM ($\uparrow\downarrow$, left panel) or FM ($\uparrow\uparrow$, right panel). Without loss of generality, we assume that the AFM state is lower in energy than the FM state by ΔE . Interestingly, it is known that an external electric field (E_{ef}) along the out of plane direction can induce a potential energy difference ΔV between the A and B layers in the *bi*-magnet. This lifts the AFM band degeneracy and consequently gives rise to an AFM to FM transition. When the E_{ext} is withdrawn, the FM phase may turn back to the AFM phase upon a small thermal perturbation, because the energy barrier E_b between the AFM and FM phases, originated from the magnetic exchange coupling (E_{xc}) and the magnetic anisotropy energy (MAE), is usually tiny (only several meV). On the other hand, in a typical FE system [Fig. 1(b)], there is a relatively large FE E_b (on the order of tens or hundreds of meV) between two equivalent phases with opposite P directions. Therefore, a sufficiently large E_{ef} is required to switch between the $P\uparrow$ and $P\downarrow$ states.

Our idea is to induce a large E_b from FE ML to the *bi*-magnet to create a sizable barrier between the AFM and FM states, whereby realizing multiferroicity in the vdW

heterojunction. As shown in Fig. 1(c), upon attaching the *bi*-magnet on a FE layer, we expect that there will be both the AFM and FM states for each P configuration. To realize the multiferroic function, the key is to achieve opposite magnetic ground states in the $P\uparrow$ and $P\downarrow$ configurations, e.g., AFM- $P\downarrow$ and FM- $P\uparrow$ [Fig. 1(c)]. As importantly, by having a large FE E_b , it will not be overly easy to switch between these two states. In the following, we will demonstrate that such an asymmetric magnetic ground state in the $P\uparrow$ and $P\downarrow$ configurations could be achieved by a mechanism of asymmetric ME coupling under the opposite P configurations.

Below, the above design principle will be demonstrated for the prototypical *bi*- $\text{CrI}_3/\text{In}_2\text{Se}_3$ system, based on extensive first-principles calculations (see computational details in Supplemental Material [34]). The intralayer E_{xc} of ML CrI_3 is always FM, while the interlayer E_{xc} can be either FM or AFM, depending on stacking sequence [44,45]. A weak interlayer E_{xc} in *bi*- CrI_3 also provides the opportunity for an AFM-FM transition via an electrostatic gating [46–48] or by applying a hydrostatic pressure [49,50]. On the other hand, the ML In_2Se_3 , consisting of [Se-In-Se-In-Se] quintuple layers, has been confirmed to be a good FE system [15,16]. As shown in Fig. 2(a), the downshift and upshift of the middle Se-2 layer will correspond to a $P\uparrow$ and $P\downarrow$ configuration, respectively.

Figure 2(b) shows ΔE between the AFM and FM states in *bi*- CrI_3 , as a result of sliding between the top and bottom layers of *bi*- CrI_3 , which could be achieved via control of pressure [49,50]. Along the sliding path, the magnetic ground state can be either FM (for $0 < x < 0.21$ and $x > 0.35$) or AFM (for $0.21 < x < 0.35$) (see the red curve), which agrees with previous calculations [45]. Importantly, this ΔE curve [Fig. 2(b)] can be down- (up-) shifted towards a lower (higher) energy position in the *bi*- $\text{CrI}_3/\text{In}_2\text{Se}_3$ under the $P\uparrow$ ($P\downarrow$) configuration, indicating the existence of a ME coupling between *bi*- CrI_3 and In_2Se_3 . The reliability of our conclusion is carefully checked (Figs. S1–S6, Tables S1–S4 [34]). Impressively, in the range of $0.16 < x < 0.37$, the *bi*- $\text{CrI}_3/\text{In}_2\text{Se}_3$ can exhibit the FM (blue curve) and AFM (green curve) ground states in the $P\uparrow$ and $P\downarrow$ configurations, respectively. For multiferroics, it is necessary to estimate E_b between the FM- $P\uparrow$ and AFM- $P\downarrow$ configurations. Without In_2Se_3 , the E_b is as small as ~ 0.65 meV/Cr, which is induced by the intrinsic E_{xc} and MAE (Fig. S7 [34]). When forming the vdW junction with In_2Se_3 , taking the typical high-temperature (HT)-phase *bi*- CrI_3 as an example [see Fig. 2(c)], a double-well potential energy surface appears, which is in line with our design principle in Fig. 1(c). Importantly, the calculated E_b between the FM- $P\uparrow$ and AFM- $P\downarrow$ configurations is as large as ~ 459.0 meV/Cr, which is sufficiently high to stabilize the FM and AFM states in different P energy wells. The magnetic ground states in the nonpolarized heterojunction (Fig. S8 [34]) is AFM with $\Delta E = 0.11$ meV/Cr. According to previous results [15,16], we estimate a small external electric field of ~ 0.72 V/nm may be applied to switch the different P configurations. The ΔE between the FM- $P\uparrow$ and AFM- $P\downarrow$ states is ~ 6.9 meV/Cr. The opposite magnetic ground states in the $P\downarrow$ and $P\uparrow$ configurations, together with the large E_b , are a strong indication that multiferroicity should be realized in this *bi*- $\text{CrI}_3/\text{In}_2\text{Se}_3$ system.

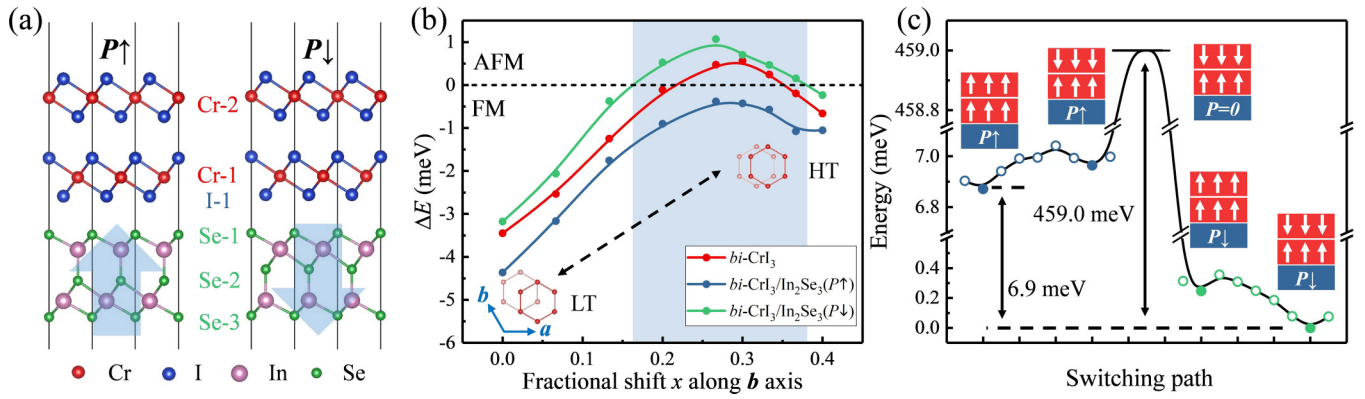


FIG. 2. Realization of vdW multiferroics in $bi\text{-CrI}_3/\text{In}_2\text{Se}_3$. (a) Side views of $bi\text{-CrI}_3/\text{In}_2\text{Se}_3$ with $P\uparrow$ (left panel) and $P\downarrow$ (right panel). (b) Energy difference (ΔE) between the FM and AFM states in the freestanding $bi\text{-CrI}_3$ and $bi\text{-CrI}_3/\text{In}_2\text{Se}_3$, as a function of the fractional shift, which is obtained by sliding the top CrI_3 layer along the b axis with respect to the bottom layer. $x = 0.0$ is the low-temperature (LT) phase, while $x = 1/3$ is the HT phase. The shaded area is where the FM- $P\uparrow$ and AFM- $P\downarrow$ states in Fig. 1(c) have been realized in $bi\text{-CrI}_3/\text{In}_2\text{Se}_3$. (c) Switching path between the FM- $P\uparrow$ and AFM- $P\downarrow$ states for the HT-phase $bi\text{-CrI}_3/\text{In}_2\text{Se}_3$. Blue and green circles are different magnetic states in the $P\uparrow$ and $P\downarrow$ configurations, respectively. When $P = 0$, the system is nonferroelectric.

It is desirable to understand the respective physical origins of the FM and AFM ground-states in the $P\uparrow$ and $P\downarrow$ configurations, which serve as the key for achieving multiferroicity in $bi\text{-CrI}_3/\text{In}_2\text{Se}_3$. Generally speaking, these systems are all semiconducting regardless of the order of P (see Fig. S9 [34]). In other words, charge transfer between In_2Se_3 and $bi\text{-CrI}_3$ is negligible, which is fundamentally different from other proposed 2D vdW multiferroic systems (overcome problem ii) [30–33]. Due to the C_{3v} crystal symmetry, the I $5p$ (Se $4p$) orbitals split into doublet $e_1(e_2)$ and singlet $a_1(a_2)$ states, which are found in $bi\text{-CrI}_3/\text{In}_2\text{Se}_3(P\uparrow)$ to be mostly located in different energies with small overlaps [see shaded areas in Fig. 3(a)]. Figure 3(b) and Fig. S10 show the orbital-projected band structure and projected densities of states (PDOS) of interfacial I-1 and Se-1 atoms, which reveals that orbital coupling (e.g., in the range of $-2 \sim 0$ eV) between the occupied I-1 $5p$ and Se-1 $4p$ states is negligible (see the wave function in Fig. S11(a) [34]). Meanwhile, the $P\uparrow$ configuration of In_2Se_3 can lead to a positive E_{ef} across $bi\text{-CrI}_3$, which can effectively lower the potential energy of the Cr-1 $3d$ states by ΔV with respect to that of the Cr-2 $3d$ states [see Fig. 3(c)]. Importantly, this ΔV will increase the strength of virtual hopping between empty Cr-1 e_g and occupied Cr-2 t_{2g} orbitals in the same spin channel [Fig. 3(a)] to result in the favored FM order in $bi\text{-CrI}_3/\text{In}_2\text{Se}_3(P\uparrow)$.

In contrast, for $bi\text{-CrI}_3/\text{In}_2\text{Se}_3(P\downarrow)$, the closer distance between Se-2 and Se-1 layers increases their orbital coupling strength, pushing the (antibonding) Se-1 states to higher energy positions. Now, the energy levels of interfacial I-1 $a_1(e_1)$ and Se-1 $a_2(e_2)$ states can have significantly larger overlaps, as indicated by the shaded areas in Fig. 3(d) [34]. Therefore, the selective orbital coupling between I-1 $5p$ and Se-1 $4p$ states is largely turned on. Meanwhile, since the I $5p$ and Cr $3d$ orbitals in $bi\text{-CrI}_3$ can strongly couple forming covalent bonds, the Se-1 $4p$ orbitals can also indirectly couple with Cr-1 $3d$ orbitals, intermediated by the I-1 $5p$ orbital. Figure 3(e) shows that there are significant triple-orbital resonances (e.g., in the range of $-2 \sim 0$ eV) among the occupied Se-1 $4p$, I-1 $5p$, and Cr-1 $3d$ states in the valence band of

$bi\text{-CrI}_3/\text{In}_2\text{Se}_3(P\downarrow)$ [see the wave function in Fig. S11(b)]. Therefore, this multiply orbital coupling will significantly lower the orbital levels of Cr-1 compared to that of Cr-2. However, the In_2Se_3 $P\downarrow$ configuration-induced negative E_{ef} would simultaneously lower the potential energy of Cr-2 $3d$ states with respect to that of Cr-1 ones, in contrast to the positive E_{ef} effect in $bi\text{-CrI}_3/\text{In}_2\text{Se}_3(P\uparrow)$. Unexpectedly, the competition between the indirect orbital coupling that lowers Cr-1 orbital levels and the negative E_{ef} effect that lowers Cr-2 orbital levels can eventually result in a rather small ΔV , as shown in Fig. 3(f). Therefore, different from $bi\text{-CrI}_3/\text{In}_2\text{Se}_3(P\uparrow)$, the virtual hopping strength between empty Cr-1 e_g and occupied Cr-2 t_{2g} orbitals cannot be noticeably enhanced [Fig. 3(d)], which prevents the AFM to FM transition.

In order to quantitatively estimate the strengths of orbital hybridizations between the two different P configurations, the Wannier function is adopted to fit the band structure and extract the hopping parameters between interfacial I-1 $5p$ and Se-1 $4p$ orbitals, as shown in Fig. S12 and Table S5 [34]. The changes of hopping parameters verify the stronger orbital coupling between In_2Se_3 and $bi\text{-CrI}_3$ in the $P\downarrow$ configuration compared to that in the $P\uparrow$ one. The above mechanism for the HT-phase $bi\text{-CrI}_3/\text{In}_2\text{Se}_3$ can be readily applied to other $bi\text{-CrI}_3/\text{In}_2\text{Se}_3$ systems with $0.16 < x < 0.37$ [Fig. 2(b)] to understand the existence of $P\uparrow$ -FM and $P\downarrow$ -AFM ground states. Although the E_{xc} strength is changed in the ranges of $0 < x < 0.16$ and $x > 0.37$, the indirect orbital coupling mechanism is not sufficiently strong to overcome the ΔE between AFM and FM states, hindering the realization of FM-AFM switching. We emphasize that the polarization switching-induced magnetic anisotropy energy change is also calculated (Table S6 [34]). Also, we emphasize that the ground states of FM- $P\uparrow$ and AFM- $P\downarrow$ maintain when the thickness of In_2Se_3 increases (Fig. S13 [34]).

This asymmetrical ME coupling can also induce different magnetic ground states in a trilayer CrI_3 ($tri\text{-CrI}_3$) system. Taking the HT-phase CrI_3 again as an example, without the In_2Se_3 layer, the ground state of $tri\text{-CrI}_3$ should exhibit an interlayer $\uparrow\downarrow\uparrow$ spin order (Fig. S14 [34]), which agrees well

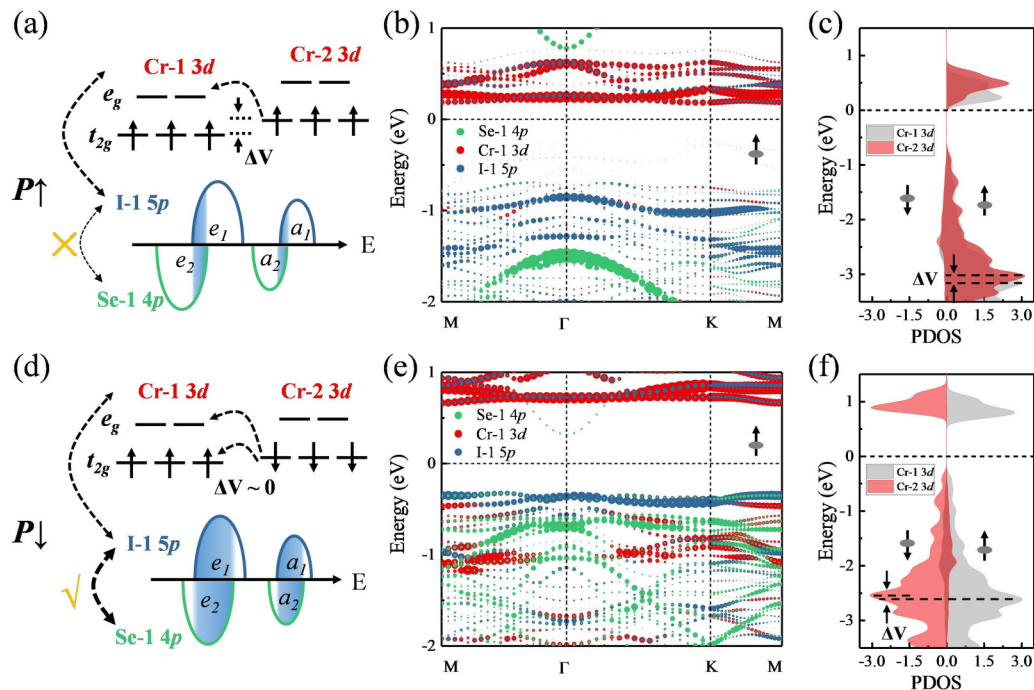


FIG. 3. Mechanism of multiferroicity in *bi*-CrI₃/In₂Se₃ where (a)–(c) are for $P\uparrow$ and (d)–(f) for $P\downarrow$. (a), (d) Schematic diagrams of orbital coupling between interfacial I-1 and Se-1 p orbitals as well as the virtual orbital hopping path between empty Cr-1 e_g and occupied Cr-2 t_{2g} orbitals. Here, ΔV is the relative energy difference between the two t_{2g} (and e_g) orbitals. In the lower part of the diagrams, $a_1(a_2)$ and $e_1(e_2)$ are the single- and doubly degenerate p orbitals of I-1 (Se-1) atoms, respectively. (b), (e) Orbital-projected band structures (spin-up channel). (c), (f) PDOS.

with experiments [51]. With the inclusion of In₂Se₃, there will be an asymmetric distribution of the ground-state spin orders between the $P\uparrow$ and $P\downarrow$ configurations, as shown in Fig. 4. In the $P\downarrow$ state, the ground-state spin order maintains as $\uparrow\downarrow\uparrow$. However, in the $P\uparrow$ state, the ground-state spin order is dramatically changed to become $\downarrow\downarrow\uparrow$. From the study of *bi*-CrI₃/In₂Se₃, we know that *bi*-CrI₃ favors the AFM (FM)

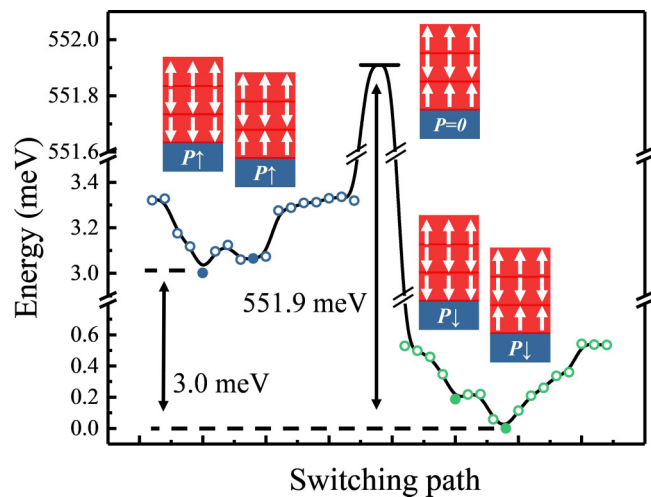


FIG. 4. Realization of vdW multiferroics in *tri*-CrI₃/In₂Se₃. Switching path of the HT-phase *tri*-CrI₃/In₂Se₃. Blue and green circles represent different magnetic states in the $P\uparrow$ and $P\downarrow$ configurations, respectively. $P = 0$ is the nonpolarized configuration.

order in the $P\downarrow$ ($P\uparrow$) configuration. Therefore, the favorable spin order of the bottom two CrI₃ layers in *tri*-CrI₃/In₂Se₃ (next to In₂Se₃) follows the same trend as in *bi*-CrI₃/In₂Se₃, which gives rise to the $\uparrow\downarrow\uparrow$ - $P\downarrow$ and $\downarrow\downarrow\uparrow$ - $P\uparrow$ ground states. Generally speaking, both *tri*-CrI₃ and *tri*-CrI₃/In₂Se₃ (Fig. S15 [34]) systems favor low-spin configurations. Together with the large $E_b \sim 551.9$ meV/Cr, the *tri*-CrI₃/In₂Se₃ system can also sustain multiferroicity with tunable interlayer spin orders, even when the total magnetic moments under different P configurations are unchanged. Furthermore, it is reasonable to expect that such exotic multiferroicity can also be realized in other multiple-layer CrI₃/In₂Se₃ systems with different layer thickness.

We would like to emphasize that our mechanism here also generally applies to design other layered double-phase multiferroic heterojunctions. As shown in Fig. S16 [34], similar AFM- $P\uparrow$ and FM- $P\downarrow$ states can also be realized in the R -type *bi*-CrBr₃/In₂Se₃ system, as a result of a similar strong asymmetrical ME coupling mechanism under different P configurations. Given that the vdW magnet, e.g., CrI₃ [11] and CrBr₃ [52], and FE ML, e.g., In₂Se₃ [15] and CuInP₂S₆ [20], have now been widely synthesized, our concept here can thus be readily tested by experiments. Therefore, in general, our findings here not only can overcome the two challenging problems (i.e., problems i and ii) existing in the current 2D multiferroics, but also can be used to design other vdW multiferroics with different components and layer thickness.

B.H. and B.Y. are thankful for the helpful discussion with Dr. B. Cui. C.Y. and B.H. were supported by the

Science Challenge Project (Grant No. TZ2016003), Grants No. NSAF U1930402, No. JCYJ 20190813164805689, and Guangdong Shenzhen Joint Key Fund (Grant No. 2019B1515120045). S.Z. was supported by U.S. DOE under

Grant No. DE-SC0002623. B.Y. was supported by the project funded by China Postdoctoral Science Foundation (Grant No. 2020M682897). All the calculations were performed at Tianhe2-JK at CSRC.

- [1] H. Schmid, *Ferroelectrics* **162**, 317 (1994).
- [2] O. Auciello, J. F. Scott, and R. Ramesh, *Phys. Today* **51**(7), 22 (1998).
- [3] S. Dong, J.-M. Liu, S.-W. Cheong, and Z. Ren, *Adv. Phys.* **64**, 519 (2015).
- [4] W. Eerenstein, N. D. Mathur, and J. F. Scott, *Nature (London)* **442**, 759 (2006).
- [5] S. Dong, H. Xiang, and E. Dagotto, *Natl. Sci. Rev.* **6**, 629 (2019).
- [6] J. Wang, J. B. Neaton, H. Zheng, V. Nagarajan, S. B. Ogale, B. Liu, D. Viehland, V. Vaithyanathan, D. G. Schlom, U. V. Waghmare, N. A. Spaldin, K. M. Rabe, M. Wuttig, and R. Ramesh, *Science* **299**, 1719 (2003).
- [7] P. Jarillo-Herrero, S. Sapmaz, C. Dekker, L. P. Kouwenhoven, and H. S. Van Der Zant, *Nature (London)* **429**, 389 (2004).
- [8] M. Wu and P. Jena, *Comput. Mol. Sci.* **8**, e1365 (2018).
- [9] Z. Guan, H. Hu, X. Shen, P. Xiang, N. Zhong, J. Chu, and C. Duan, *Adv. Electron. Mater.* **6**, 1900818 (2019).
- [10] C. Gong, L. Li, Z. Li, H. Ji, A. Stern, Y. Xia, T. Cao, W. Bao, C. Wang, Y. Wang, Z. Q. Qiu, R. J. Cava, S. G. Louie, J. Xia, and X. Zhang, *Nature (London)* **546**, 265 (2017).
- [11] B. Huang, G. Clark, E. Navarro-Moratalla, D. R. Klein, R. Cheng, K. L. Seyler, D. Zhong, E. Schmidgall, M. A. McGuire, D. H. Cobden, W. Yao, D. Xiao, P. Jarillo-Herrero, and X. Xu, *Nature (London)* **546**, 270 (2017).
- [12] M. Bonilla, S. Kolekar, Y. Ma, H. C. Diaz, V. Kalappattil, R. Das, T. Eggers, H. R. Gutierrez, M. H. Phan, and M. Batzill, *Nat. Nanotechnol.* **13**, 289 (2018).
- [13] Z. Fei, B. Huang, P. Malinowski, W. Wang, T. Song, J. Sanchez, W. Yao, D. Xiao, X. Zhu, A. F. May, W. Wu, D. H. Cobden, J. H. Chu, and X. Xu, *Nat. Mater.* **17**, 778 (2018).
- [14] C. Gong and X. Zhang, *Science* **363**, eaav4450 (2019).
- [15] W. Ding, J. Zhu, Z. Wang, Y. Gao, D. Xiao, Y. Gu, Z. Zhang, and W. Zhu, *Nat. Commun.* **8**, 14956 (2017).
- [16] C. Cui, W. J. Hu, X. Yan, C. Addiego, W. Gao, Y. Wang, Z. Wang, L. Li, Y. Cheng, P. Li, X. Zhang, H. N. Alshareef, T. Wu, W. Zhu, X. Pan, and L. J. Li, *Nano Lett.* **18**, 1253 (2018).
- [17] J. Xiao, H. Zhu, Y. Wang, W. Feng, Y. Hu, A. Dasgupta, Y. Han, Y. Wang, D. A. Muller, L. W. Martin, P. A. Hu, and X. Zhang, *Phys. Rev. Lett.* **120**, 227601 (2018).
- [18] A. Chandrasekaran, A. Mishra, and A. K. Singh, *Nano Lett.* **17**, 3290 (2017).
- [19] A. Belianinov, Q. He, A. Dziaugys, P. Maksymovych, E. Eliseev, A. Borisevich, A. Morozovska, J. Banys, Y. Vysochanskii, and S. V. Kalinin, *Nano Lett.* **15**, 3808 (2015).
- [20] F. Liu, L. You, K. L. Seyler, X. Li, P. Yu, J. Lin, X. Wang, J. Zhou, H. Wang, H. He, S. T. Pantelides, W. Zhou, P. Sharma, X. Xu, P. M. Ajayan, J. Wang, and Z. Liu, *Nat. Commun.* **7**, 12357 (2016).
- [21] R. Fei, W. Kang, and L. Yang, *Phys. Rev. Lett.* **117**, 097601 (2016).
- [22] K. Chang, J. Liu, H. Lin, N. Wang, K. Zhao, A. Zhang, F. Jin, Y. Zhong, X. Hu, W. Duan, Q. Zhang, L. Fu, Q.-K. Xue, X. Chen, and S.-H. Ji, *Science* **353**, 274 (2016).
- [23] K. Liu, J. Lu, S. Picozzi, L. Bellaiche, and H. Xiang, *Phys. Rev. Lett.* **121**, 027601 (2018).
- [24] C. Huang, Y. Du, H. Wu, H. Xiang, K. Deng, and E. Kan, *Phys. Rev. Lett.* **120**, 147601 (2018).
- [25] M. Xu, C. Huang, Y. Li, S. Liu, X. Zhong, P. Jena, E. Kan, and Y. Wang, *Phys. Rev. Lett.* **124**, 067602 (2020).
- [26] J. Qi, H. Wang, X. Chen, and X. Qian, *Appl. Phys. Lett.* **113**, 043102 (2018).
- [27] H. Tan, M. Li, H. Liu, Z. Liu, Y. Li, and W. Duan, *Phys. Rev. B* **99**, 195434 (2019).
- [28] A. K. Geim and I. V. Grigorieva, *Nature (London)* **499**, 419 (2013).
- [29] K. S. Novoselov, A. Mishchenko, A. Carvalho, and A. H. Castro Neto, *Science* **353**, aac9439 (2016).
- [30] Y. Zhao, J. J. Zhang, S. Yuan, and Z. Chen, *Adv. Funct. Mater.* **29**, 1901420 (2019).
- [31] Y. Lu, R. Fei, X. Lu, L. Zhu, L. Wang, and L. Yang, *ACS Appl. Mater. Interfaces* **12**, 6243 (2020).
- [32] W. Sun, W. Wang, D. Chen, Z. Cheng, and Y. Wang, *Nanoscale* **11**, 9931 (2019).
- [33] Z. Li and B. Zhou, *J. Mater. Chem. C* **8**, 4534 (2020).
- [34] See Supplemental Material at <http://link.aps.org/supplemental/10.1103/PhysRevB.103.L201405> for computational methods, reliability of the parameters, switching paths of freestanding *bi*-CrI₃ and *tri*-CrI₃, electronic structure of *bi*-CrI₃, In₂Se₃, *bi*-CrI₃/In₂Se₃ (*P*↑), *bi*-CrI₃/In₂Se₃ (*P*↓), and *bi*-CrI₃/*bi*-In₂Se₃, real part of wave functions, magnetic anisotropy energy, hopping parameter with Wannier fit, and the corresponding results of *R*-type *bi*-CrBr₃, which includes Refs. [35–43].
- [35] G. Kresse and J. Furthmüller, *Comput. Mater. Sci.* **6**, 15 (1996).
- [36] J. P. Perdew, K. Burke, and M. Ernzerhof, *Phys. Rev. Lett.* **77**, 3865 (1996).
- [37] J. Klimeš, D. R. Bowler, and A. Michaelides, *Phys. Rev. B* **83**, 195131 (2011).
- [38] J. Klimeš, D. R. Bowler, and A. Michaelides, *J. Phys.: Condens. Matter* **22**, 022201 (2009).
- [39] S. L. Dudarev, G. A. Botton, S. Y. Savrasov, C. J. Humphreys, and A. P. Sutton, *Phys. Rev. B* **57**, 1505 (1998).
- [40] J. Zhang, B. Zhao, T. Zhou, Y. Xue, C. Ma, and Z. Yang, *Phys. Rev. B* **97**, 085401 (2018).
- [41] S. W. Jang, M. Y. Jeong, H. Yoon, S. Ryee, and M. J. Han, *Phys. Rev. Materials* **3**, 031001(R) (2019).
- [42] B. S. Yang, J. Zhang, L. N. Jiang, W. Z. Chen, P. Tang, X.-G. Zhang, Y. Yan, and X. F. Han, *Phys. Rev. B* **95**, 174424 (2017).
- [43] X. Huang, G. Li, C. Chen, X. Nie, X. Jiang, and J.-M. Liu, *Phys. Rev. B* **100**, 235445 (2019).
- [44] P. Jiang, C. Wang, D. Chen, Z. Zhong, Z. Yuan, Z.-Y. Lu, and W. Ji, *Phys. Rev. B* **99**, 144401 (2019).

- [45] N. Sivadas, S. Okamoto, X. Xu, C. J. Fennie, and D. Xiao, *Nano Lett.* **18**, 7658 (2018).
- [46] S. Jiang, J. Shan, and K. F. Mak, *Nat. Mater.* **17**, 406 (2018).
- [47] B. Huang, G. Clark, D. R. Klein, D. MacNeill, E. Navarro-Moratalla, K. L. Seyler, N. Wilson, M. A. McGuire, D. H. Cobden, D. Xiao, W. Yao, P. Jarillo-Herrero, and X. Xu, *Nat. Nanotechnol.* **13**, 544 (2018).
- [48] S. Jiang, L. Li, Z. Wang, K. F. Mak, and J. Shan, *Nat. Nanotechnol.* **13**, 549 (2018).
- [49] T. Song, Z. Fei, M. Yankowitz, Z. Lin, Q. Jiang, K. Hwangbo, Q. Zhang, B. Sun, T. Taniguchi, K. Watanabe, M. A. McGuire, D. Graf, T. Cao, J. H. Chu, D. H. Cobden, C. R. Dean, D. Xiao, and X. Xu, *Nat. Mater.* **18**, 1298 (2019).
- [50] T. Li, S. Jiang, N. Sivadas, Z. Wang, Y. Xu, D. Weber, J. E. Goldberger, K. Watanabe, T. Taniguchi, C. J. Fennie, K. Fai Mak, and J. Shan, *Nat. Mater.* **18**, 1303 (2019).
- [51] T. Song, X. Cai, M. W.-Y. Tu, X. Zhang, B. Huang, N. P. Wilson, K. L. Seyler, L. Zhu, T. Taniguchi, K. Watanabe, M. A. McGuire, D. H. Cobden, D. Xiao, W. Yao, and X. Xu, *Science* **360**, 1214 (2018).
- [52] W. Chen, Z. Sun, Z. Wang, L. Gu, X. Xu, S. Wu, and C. Gao, *Science* **366**, 983 (2019).